PHYSICAL REVIEW FLUIDS **7**, 114603 (2022)

Editors' Suggestion

# Meandering features of wall-attached structures in turbulent boundary layer

Jinyul Hwang [1,*] and Jae Hwa Lee [2,†]

[1] *School of Mechanical Engineering, Pusan National University, 2 Busandaehak-ro 63beon-gil Geumjeong-gu, Busan 46241, Korea*

[2] *Department of Mechanical Engineering, UNIST, 50 UNIST-gil, Ulsan 44919, Korea*

(Received 8 October 2021; accepted 18 October 2022; published 14 November 2022)

In wall turbulence, meandering behaviors of large-scale structures observed in the logarithmic layer are a crucial spatial feature to understand the spatial organization of these structures and to improve the structure-based turbulence model. These structures extend from the near-wall region to the edge of boundary layers ($\delta$). Thus, their meandering motions leave an imprint on the two-point turbulence statistics across the flow, especially in the logarithmic region. Herein, we demonstrate the influence of the meandering motions of wall-attached structures on the two-point correlation and the premultiplied two-dimensional spectra by analyzing the direct numerical simulation data of the turbulent boundary layer at $\mathrm{Re}_\tau \approx 1000$. The meandering magnitudes of wall-attached structures increase with their height ($l_y$) but significantly differ among the identified structures even at a given $l_y$. In addition, the wall-attached structures of streamwise velocity fluctuations ($u$) are found to be aligned along with a preferred spanwise offset regardless of the meandering motion. This feature is confirmed through the conditional two-point correlations of $u$ within the meandering structures, which leads to a distinct X pattern in the logarithmic region. We further examine the spectral behavior of the meandering structures across the streamwise and spanwise wavelengths ($\lambda_x$ and $\lambda_z$, respectively) through the premultiplied two-dimensional spectra. With increasing meandering magnitudes, the energy spectra are more inclined to the $\lambda_z$ direction. Furthermore, the energy spectra of the strong meandering structures are bounded by a linear relationship $\lambda_x \sim \lambda_z$ over the large-scale range, reminiscent of self-similar scaling predicted by the attached-eddy hypothesis. In particular, the upper bound is aligned along $\lambda_x \approx 2\lambda_z$ over $\lambda_z > \delta$, which is absent in the energy spectral of the total $u$. This result reveals that the meandering motions allow the large-scale structures to contain wide spanwise scale energy that is self-similar in the logarithmic region. Finally, a discussion on the near-wall parts of the meandering structures is given with an emphasis on Townsend's inactive eddies.

DOI: 10.1103/PhysRevFluids.7.114603

## I. INTRODUCTION

Wall-bounded turbulent flows are characterized by a broad range of turbulence motions that maintain their spatial and temporal coherence, so-called eddies or coherent structures [1–3]. Due to their coherence, these organized motions play an essential role in sustaining turbulence by producing turbulent kinetic energy and mass, momentum, or heat transport.

A noteworthy feature in the near-wall region is the presence of low-speed streaks in which the streamwise velocity is lower than the mean velocity at a given wall-normal location [4]. The

*jhwang@pusan.ac.kr
†jhlee06@unist.ac.kr

 

low-speed streaks are flanked by vortical structures, and these near-wall coherent motions interact with each other through a self-sustaining cycle [5–7]. The sizes of the near-wall coherent structures are an order of the viscous lengthscale $\delta_\nu = \nu/u_\tau$, where $\nu$ is the kinematic viscosity and $u_\tau$ is the friction velocity. In addition, low-speed streaks exhibit a sinuous (or meandering) motion that is responsible for the regeneration of the vortical structures.

Above the buffer layer, there are long low-speed regions whose lengthscales are an order of the flow thickness $\delta$, where $\delta$ is the 99% boundary-layer thickness, the channel half-height, or the pipe radius. These large-scale features are related to the bulges observed in the outer layer [2,8–10] since the two-point correlation of the streamwise velocity indicates that they are correlated far above the wall [11,12]. In addition, long low-speed regions flanked by high-speed regions are found in the wall-parallel plane of the logarithmic layer [13–15]. Furthermore, long low-speed streaks in the logarithmic layer extend along the streamwise direction at very large scales of $O(10\delta - 20\delta)$—the so-called very-large-scale motion [16] or superstructures [13] or global modes [17]. Given that these large-scale structures significantly contribute to the Reynolds shear stress in the outer region [15,17–25] and influence the near-wall region via the superposition [13,26,27] and the amplitude modulation [28–32], it is crucial to understand their spatial organization in wall-bounded turbulent flows. Furthermore, the near-wall velocity signals can be predicted by considering the influence of large scales on the near-wall region [33–35].

A robust feature of large-scale streaks in the logarithmic region is that they significantly meander along the streamwise direction in the turbulent boundary layer (TBL) and internal flows [13,14]. Moreover, similar large-scale meandering patterns are observed in the near-wall region, representing a footprint of the large-scale streaks [13,26], which is in turn related to inner-outer interactions [24,28,32,36–38]. Using a volumetric conditional average of the velocity fields based on the large-scale filtered low skin-friction events, Ref. [39] showed that the large-scale meandering event in the near-wall region is associated with large-scale streaks in the logarithmic region, and the magnitude of the associated streamwise velocity fluctuations is greater than that of the straight large-scale event. In the logarithmic region, Ref. [36] extracted one very long meandering streak whose streamwise length is approximately $20\delta$, and it showed that such a long streak is vertically connected to a group of near-wall low-speed streaks. Furthermore, the near-wall streaks were organized into a similar meandering pattern of the $20\delta$-long meandering streak. In this regard, a meandering feature of large-scale structures is crucial to understanding the multiscale nature of wall-bounded turbulent flows.

The meandering motion of large-scale structures originally received attention because of a shortening of streamwise lengthscales in Ref. [13]. By synthesizing sinusoidal streaks, they showed that the streak meandering could contaminate statistical lengthscales shown in the two-point correlation and the premultiplied energy spectra. Additionally, a distinctive X pattern in the two-point correlation of the streamwise velocity fluctuations ($u$) was observed in the low level of the correlations. Such a feature was reproduced through synthetic meandering streaks. This observation reflects that the meandering nature of low- and high-speed regions in the logarithmic layer contributes to the X-shaped correlations. Reference [40] also found a similar flow pattern of the two-point correlation in the turbulent pipe flow. They pointed out that this behavior is not a consequence of noise or lack of convergence. Instead, it is because of a preferred spanwise offset of large-scale meandering structures called a helical angle in the streamwise-azimuthal plane. Through a proper orthogonal decomposition (POD), the helical angle of dominant modes was $4^\circ$–$8^\circ$ with respect to the streamwise direction. In addition, they speculated that a streamwise alignment of large-scale structures along with the helical angle leads to the formation of very-large-scale motions.

In structural aspects, the meandering behavior of large-scale structures along a preferred spanwise offset can be used to improve the coherent structure-based models in wall turbulence. Specifically, the attached eddy model (AEM) proposed by Refs. [41,42] can be enhanced by considering the spatial organization of large-scale structures. Reference [43] measured the meandering behavior along the wall-normal direction and proposed a representative structure of large-scale structures by considering their meandering motion. Reference [44] found that the X-shaped pattern in the two-point correlation can be reproduced through the AEM configuration with helical angles. In addition, Ref. [45] reported a better prediction of the wall-normal variation of the streamwise lengthscale in the two-point correlation using a modified AEM, which includes the meandering behavior. To further improve the AEM, it would be reasonable to scrutinize the spectral contribution of turbulence motions contained within the long meandering structures observed in the instantaneous flow fields.

As described earlier, large-scale meandering structures extend from the near-wall region to the edge of the boundary layer. In other words, the height of the large-scale structures is on the order of $\delta$. Recently, Ref. [46] extracted three-dimensional $u$ structures in the instantaneous flow fields and showed that these structures could be classified into wall-attached and wall-detached groups analogously to those for the vortical [47] and the Reynolds shear stress structures [48]. Moreover, wall-attached $u$ structures with a height of $O(\delta)$ extend along with the streamwise direction $O(6\delta)$, reminiscent of very-large-scale motions or superstructures. Given that these structures are scaled with the outer lengthscale in TBL [46,49], pipe flow [50–52], and open channel flow over wavy wall [53], they can be interpreted as non-self-similar structures [54,55]. In particular, it was observed that these structures significantly meander along the streamwise direction [46,55]. Moreover, given that their heights are $O(\delta)$, their meandering behaviors leave an imprint across the logarithmic region. Hence, extracting instantaneous $u$ signals within the meandering structures can enable the investigation of the turbulence motions associated with the meandering structures without artificially generating $u$ streaks.

Therefore, this study aims to elucidate the influence of meandering features of wall-attached $u$ structures on turbulence statistics, emphasizing the conditional two-point correlation and their spectral characteristics in the two-dimensional spectrum. We analyze the direct numerical simulation (DNS) dataset of a zero-pressure-gradient TBL at $\mathrm{Re}_\tau \approx 1000$. We will demonstrate the influence of wavering behaviors of the identified structures on a distinctive X pattern in the two-point correlation. In addition, the two-dimensional energy spectrum of $u$ is analyzed by conditionally sampling $u$ contained within meandering structures. This analysis facilitates the examination of the spectral behavior of the turbulence motions associated with the meandering structures across the streamwise and spanwise wavelengths.

This paper is organized as follows. First, a brief explanation of the present DNS data is provided in Sec. II A. Then, in Sec. II B, we briefly describe the identification of wall-attached $u$ structures in instantaneous flow fields, and we introduce a method of measuring the meandering motions of the identified structures. Next, the statistical properties of meandering wall-attached $u$ structures are presented in Sec. III A. We then examine the conditional two-point correlations of meandering structures in Sec. III B, and the associated two-dimensional energy spectrum in Sec. III C. In Sec. III D, we discuss the near-wall footprints of the extracted meandering structures. Finally, we provide conclusions of the main findings in Sec. IV.

## II. TBL DNS DATA AND METHOD FOR MEASURING MEANDERING BEHAVIOR

### A. TBL DNS data

We use data from the DNS of a zero-pressure-gradient TBL by Refs. [32,38]. The continuity and Navier-Stokes equations for incompressible flow were numerically solved using the fractional method of Ref. [56]. In this study, the streamwise, wall-normal, and spanwise directions are denoted by $x$, $y$, and $z$, respectively, and the corresponding velocities are $\tilde{u}$, $\tilde{v}$, and $\tilde{w}$. Capital letters indicate the mean velocities ($U$, $V$, and $W$), and the lowercase letters denote the fluctuating velocity components ($u$, $v$, and $w$). The superscript $+$ indicates quantities normalized by the viscous scales (i.e., friction velocity $u_\tau$ and kinematic viscosity $\nu$), and an angled bracket $\langle\cdot\rangle$ is used to denote ensemble averaging. The computational domain size is $2300\delta_0 \times 100\delta_0 \times 100\delta_0$ along $x$, $y$, and $z$, where $\delta_0$ denotes the inlet boundary layer thickness. A staggered grid is employed with $13\,313 \times 541 \times 769$ grid points. The friction Reynolds number reaches up to $\mathrm{Re}_\tau \equiv u_\tau\delta/\nu \approx 1040$.

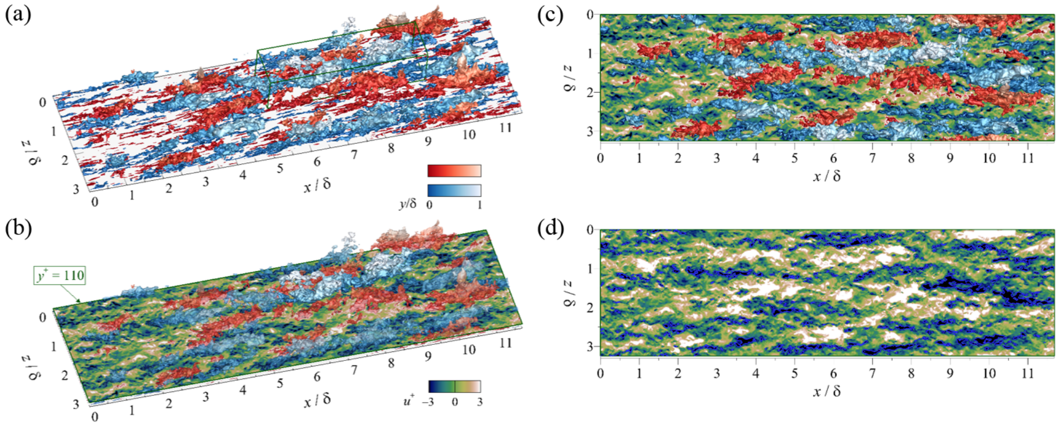


FIG. 1. (a) Isosurfaces of wall-attached structures of streamwise velocity fluctuations ($u = -1.5u_{\mathrm{rms}}$ and $1.5u_{\mathrm{rms}}$) in an instantaneous flow field. (b) Transparent isosurfaces of wall-attached structures with the wall-parallel plane $y^+ = 110$ at the same instance as the frame (a); a sample structure of negative $u$ enclosed by the green box in (a) is highlighted. (c) A top view of the instantaneous flow field in (b). (d) Contours of $u$ in the wall-parallel plane at $y^+ = 110$. The blue line is a slice of the wall-attached negative-$u$ structures.

The uniform grid spacing corresponds to $\Delta x^+ = 5.49$ and $\Delta z^+ = 4.13$ in the streamwise and spanwise directions, respectively, and the minimum and maximum grid sizes in the wall-normal direction are $\Delta y^+_{\mathrm{min}} = 0.159$ and $\Delta y^+_{\mathrm{max}} = 9.56$. The time step is $\Delta t^+ = 0.0504$; details of the DNS and the validation are provided in the study by Ref. [32]. We examine 2430 instantaneous flow fields with the subdomain size of $11.7\delta \times 1.6\delta \times 3.2\delta$ in $x$, $y$, $z$ directions. Here, $\delta$ is taken at the middle of the subdomain where the friction Reynolds number is $\mathrm{Re}_\tau = 980$. The present TBL is spatially developing along the streamwise direction; however, the Reynolds-number effect is negligible as $\mathrm{Re}_\tau$ varies from 931 to 1039 over the subdomain.

### B. Method for measuring meandering behavior

To investigate the long meandering behavior of wall-attached $u$ structures, cluster detection and conditional sampling techniques are applied to the three-dimensional instantaneous flow fields. We define the clusters as the contiguous points of intense positive or negative $u$ regions, i.e., $u > 1.5u_{\mathrm{rms}}$ or $u < -1.5u_{\mathrm{rms}}$, where $u_{\mathrm{rms}}$ is the standard deviation of the streamwise velocity. Further detailed descriptions of the identification methodology can be found in Ref. [46]. Figure 1 shows an instantaneous visualization of the three-dimensional $u$ clusters whose minimum distance from the wall ($y_{\mathrm{min}}$) is close to zero (i.e., $y^+_{\mathrm{min}} \approx 0$). These clusters are classified as wall-attached structures because they physically adhere to the wall. As seen, we can observe wall-attached $u$ structures with a wide range of heights from the near-wall region to the outer region. There are many tiny objects that resemble near-wall streaklike structures within the buffer layer. On the other hand, we can also see very large objects that extend beyond the boundary-layer thickness. In the present study, we focus on the identified structures that extend beyond $y^+ = 100$; i.e., the heights of the objects ($l_y$) are larger than 100 wall units. Figure 1(b) displays a prospective view of the flow field with the wall-parallel plane of $u$ contours at $y^+ = 110$. All the structures with $l_y^+$ less than 110 are buried beneath the $x$-$z$ plane. Thus, the tall wall-attached structures with $l_y^+ > 110$ can be observed as shown in the top view [Fig. 1(c)]. As shown in Fig. 1(d), these structures meander along the streamwise direction, especially across the logarithmic region, implying that they are responsible for very long meandering signatures of positive and negative $u$ in the logarithmic and

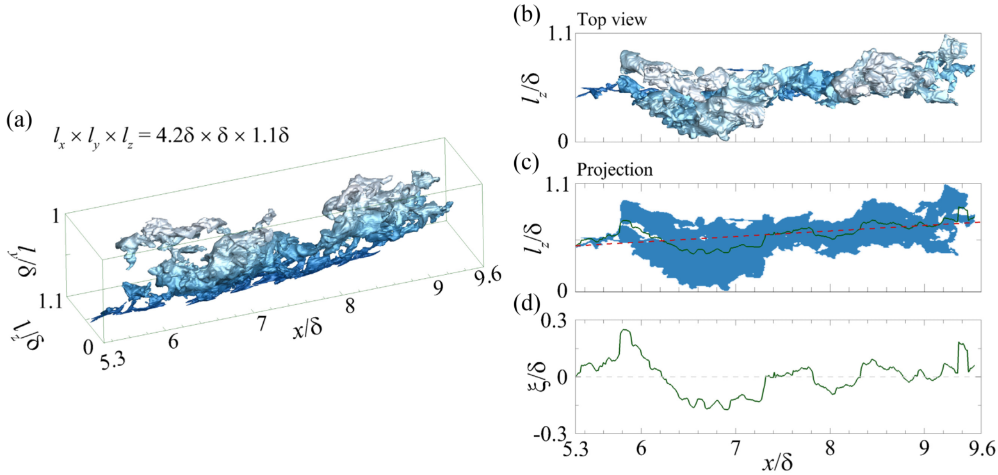


FIG. 2. Instantaneous visualization of highly meandering wall-attached structure (negative $u$) extracted from Fig. 1: (a) perspective view and (b) top view. (c) The projection (blue region) of the identified structure onto the wall. Here, the green solid line represents the spine of the projection area ($z_{\text{spine}}$), and the red dotted line denotes the linear fit of the spine ($z_{\text{fit}}$). (d) The variation of the spine about the linear fit ($\xi = z_{\text{spine}} - z_{\text{fit}}$). The meandering magnitude is $\xi_2/\delta = 0.26$.

outer regions [13,14]. However, the degree of meandering tendency in each structure seems to be remarkably different.

To quantify this wavy motion, we measure the meandering magnitudes of individual $u$ structures. Figure 2(a) illustrates a sample streaky structure of negative $u$ that is located over $5.3 < x/\delta < 9.6$ and $0.5 < z/\delta < 1.6$ in Fig. 1. Herein, the sizes of each structure correspond to those of the bounding box. The length ($l_x$), height ($l_y$), and width ($l_z$) of the sample structures in Fig. 2(a) are $4.2\delta$, $\delta$, and $1.1\delta$, respectively, representing a very large streaky $u$ structure. Figure 2(b) shows a top view of the extracted structure. As seen, the structure significantly meanders along the streamwise direction. We measure the degree of meandering motion based on the projected area onto the wall [Fig. 2(c)]. The spine location ($z_{\text{spine}}$) of the projected area, denoted by the green solid line in Fig. 2(c), is defined by measuring the mean spanwise location of the projected area at a given streamwise location, that is, $z_{\text{spine}} = (z_{\max} + z_{\min})/2$, where $z_{\max}$ and $z_{\min}$ are the maximum and minimum spanwise location of the projected area at every streamwise position. Then, the linear fit $z_{\text{fit}}$, denoted by the red dashed line in Fig. 2(c), is obtained from $z_{\text{spine}}$. The waviness of $z_{\text{spine}}$ ($\xi$) is defined as the difference in the spanwise location between $z_{\text{fit}}$ and $z_{\text{spine}}$ (i.e., $\xi = z_{\text{spine}} - z_{\text{fit}}$) and is shown in Fig. 2(d). This methodology is similar to the work of Ref. [43], except that this study quantifies the waviness of three-dimensional $u$ structures without applying a Gaussian filter. On the basis of the variation of the spine location with respect to its linear fit, we can quantify the meandering magnitude of each object by measuring the root mean square of $\xi$ (i.e., $\xi_2$). Hence, the meandering magnitude of the $k$th object is defined as

$$\xi_2(k) = \left( \frac{1}{l_x(k)} \int_{x_{\min}}^{x_{\max}} \xi^2(x;k)dx \right)^{1/2}, \tag{1}$$

where $x_{\min}$ and $x_{\max}$ denote the minimum and maximum streamwise location of the $k$th object, and $l_x = x_{\max} - x_{\min}$. Here, $k$ is the index of the identified structures. The identified object in Fig. 2 significantly meanders with $\xi_2/\delta = 0.26$. In addition, the angle of linear fit represents a spanwise-inclined nature of streaky structures. In particular, the spanwise inclination angle in Fig. 2 is approximately $3.5^{\circ}$, which is similar to that of VLSM in pipe flow [40,44]. The identification

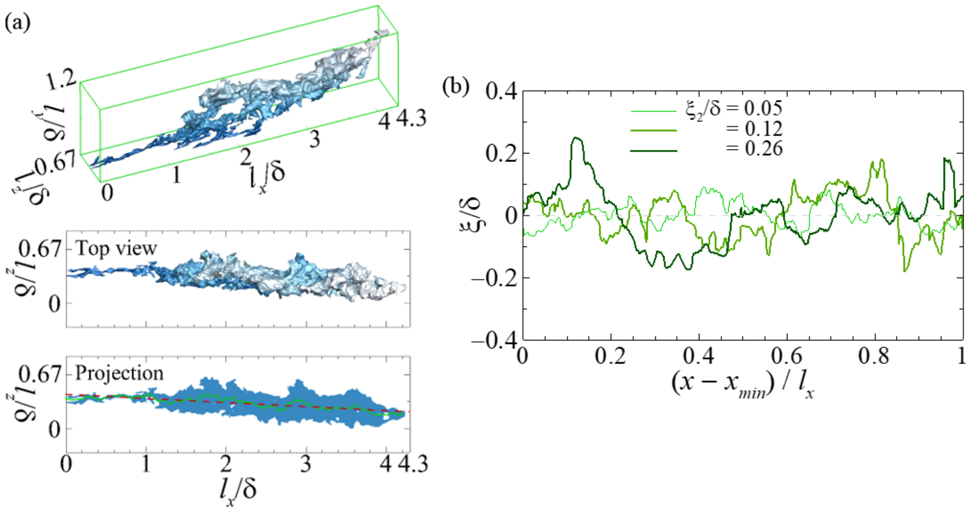


FIG. 3. (a) Instantaneous visualization of the wall-attached structure of negative $u$ with $\xi_2/\delta = 0.05$. (b) The variations of $\xi$ with different meandering magnitudes according to $(x - x_{\min})/l_x$.

method introduced in the present work measures the physical lengthscales ($l_x$, $l_y$, and $l_z$) and $\xi_2$ of each structure in instantaneous flow fields. This method allows us to sample the velocity information conditionally based on the structural features (i.e., meandering motions) of the instantaneous coherent structures.

Figure 3(a) is an example of a weak meandering structure with $\xi_2/\delta = 0.05$. The length and height of this object are $l_x/\delta = 4.3$ and $l_y/\delta = 1.2$, respectively, which are similar to those in Fig. 2, but the meandering magnitude is extremely small. In other words, the fluctuation of the spine location is weak, indicating that the structure is straight with respect to the linear fit of the spine ($z_{\text{fit}}$). Interestingly, the spanwise inclination angle of $z_{\text{fit}}$ is approximately 3.0°, which is an analogous manner to that for the severely meandering structure in Fig. 2. This result may indicate that tall wall-attached $u$ structures [i.e., $l_y \sim O(\delta)$] possess a similar spanwise inclination angle regardless of the meandering magnitudes.

To compare the $\xi$ signal with a different streamwise length of wall-attached $u$ structures, we plot the variation of $\xi$ according to $(x - x_{\min})/l_x$ in Fig. 3(b). Here, $x_{\min}$ is the most upstream position of each object. There are three cases with different $\xi_2$. The variations with $\xi_2/\delta = 0.26$ and 0.05 are obtained from the sample structures shown in Figs. 2(d) and 3(a), respectively. It is evident that the signal of $\xi_2/\delta = 0.26$ (dark green) fluctuates from $-0.2$ to $+0.2$, whereas the fluctuation magnitude of $\xi_2/\delta = 0.05$ (light green) is less than 0.1. This level of waviness is also related to the spanwise size of each object. For example, the width of a highly meandering structure [Fig. 2(a)] is $l_z = 1.1\delta$, which is much larger than that of a less meandering one [Fig. 3(a)] with $l_z = 0.67\delta$. Notably, the spanwise inclination angle—the so-called helical angle [40]—can also reflect the meandering motions of large-scale structures. In particular, given the streamwise concatenation of large-scale structures [16,40,44], the spanwise offset of each large-scale structure can lead to meandering flow patterns for very long structures in the logarithmic region [43]. In the present work, we define the meandering magnitude ($\xi_2$) as the waviness of al structure with respect to its spanwise inclination, as described in Fig. 2. Hereafter, we will refer to the spanwise inclination as the helical angle to distinguish it from $\xi_2$, as defined in the present work. In the next section, the influence of the meandering magnitudes on the spatial organization of wall-attached $u$ structures is examined statistically by measuring the sizes of all the identified structures in the TBL data.

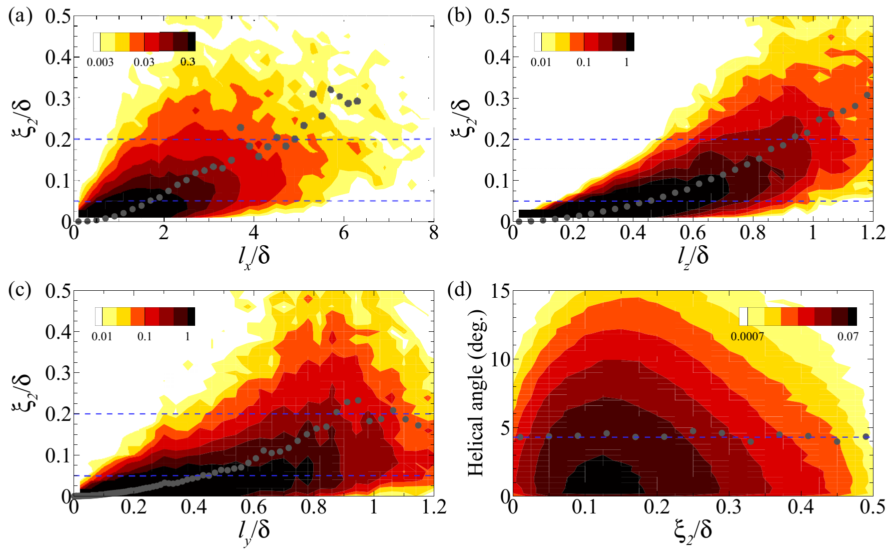


FIG. 4. Joint probability density functions (PDFs) of the sizes of the meandering structures. (a) Streamwise length ($l_x$) of the structures as a function of the meandering magnitude ($\xi_2$). (b) Spanwise width ($l_z$) of the structures as a function of $\xi_2$. (c) Wall-normal height ($l_y$) of the structures as a function of $\xi_2$. (a)–(c) The inserted dot indicates the mean meandering magnitude $\langle\xi_2\rangle$ according to $l_x$, $l_z$, or $l_y$. The horizontal dashed lines represent $\xi_2/\delta = 0.05$ and 0.2. (d) Joint PDF of the helical angle as a function of $\xi_2$. The inserted cycle denotes the variation of the mean helical angle according to $\xi_2$. The horizontal dashed line represents the helical angle of 4.3°. The contour levels are logarithmically distributed.

## III. RESULTS AND DISCUSSION

### A. Size of meandering structures

To further investigate the relation between the sizes of the identified structures and the meandering motions, we plot the joint probability density functions (PDFs) of the sizes of the meandering structures in Figs. 4(a)–4(c). As discussed above, the identified objects show a wide range of $\xi_2$ at a given size. In addition, $\xi_2$ becomes widely distributed with increasing $l_x$, $l_z$, or $l_y$. In each panel, the inserted cycles represent the variation of the mean meandering magnitudes $\langle\xi_2\rangle$. As seen, the variations of $\langle\xi_2\rangle$ increase gradually, indicating that the mean level of waviness is greater in larger structures. However, $\langle\xi_2\rangle$ flatten for tall structures ($l_y > 0.8\delta$) in Fig. 4(c), which is similar to the results in low-momentum regions [43]. In particular, $\langle\xi_2\rangle$ closes to $0.2\delta$ (indicated by horizontal dashed line) for $l_y > 0.8\delta$. The joint PDF in Fig. 4(c) shows that the wall-normal height of the structures with $\xi_2/\delta > 0.2$ is greater than $0.3\delta$. This indicates that the wall-attached structures with strong meandering motion extend beyond the logarithmic region. Given that these tall structures are elongated along the streamwise direction [46,51,55], they are related to very long meandering features observed in the logarithmic region; i.e., very-large-scale motions [16] or superstructures [13]. Interestingly, the minimum streamwise length of the structures with $\xi_2/\delta > 0.2$ is approximately equal to $\delta$ [Fig. 4(a)], which corresponds to the nominal criteria for distinguishing large-scale motions [2,13,29]. Moreover, the mean meandering magnitudes $\langle\xi_2\rangle$ becomes greater than $0.2\delta$ for $l_x > 3$–$4\delta$ similar to the streamwise length that differentiates large-scale motions and very-large-scale motions [20–22,24,40]. Hence, the strong meandering ($\xi_2/\delta \geqslant 0.2$) wall-attached structures can be considered large-scale motions or very-large-scale motions regarding the streamwise length.

Note that here we focus on the structural characteristic of meandering structures and demonstrate the relationship between the physical sizes of the identified structures and their meandering magnitudes. Given that attached eddies in the logarithmic region sustain themselves similar to the self-sustaining cycle of near-wall coherent structures [36], it would be interesting in future efforts to explore the time history of the meandering magnitude by tracking wall-attached structures and surrounding vortical structures simultaneously. Furthermore, since very long $u$ structures experience a rapid sinuous meandering motion and regenerate vortical structures [36], a wide distribution of the meandering magnitudes at a given size, observed in Figs. 4(a)–4(c), illustrates wall-attached structures at different stages of sinuous meandering motion.

In this study, for simplicity, we classify wall-attached $u$ structures into the following three categories to examine the influence of the meandering magnitudes on the turbulence statistics: weak meandering structures ($\xi_2/\delta < 0.05$); mild meandering structures ($0.05 \leqslant \xi_2/\delta < 0.2$); and strong meandering structures ($\xi_2/\delta \geqslant 0.2$). The identified structures within the lowest $\xi_2$ range of $\xi_2/\delta < 0.05$ account for 80% of the total number of the structures that cross the logarithmic region (i.e., $l_y^+ > 100$). In Fig. 4(c), $l_y$ of weak meandering structures are distributed from the near-wall region to the edge of the boundary layer. As shown in Figs. 4(a) and 4(b), most of these structures have small $l_x$ and $l_z$, containing 21% of the total volume of the identified structures with $l_y^+ > 100$. In contrast, for strong meandering structures ($\xi_2/\delta \geqslant 0.2$), they contain 28% of the volume even though they occupy 2% of the total number of the structures with $l_y^+ > 100$. In other words, the wall-attached meandering $u$ structures that extend beyond the logarithmic region occupy a large volume of intense $u$ regions throughout the boundary layer. Note that the volume of each structure was obtained by computing all the contiguous points within each object.

Figure 4(d) shows the joint PDF of the helical angle according to $\xi_2$. The helical angle of each structure is obtained from the spanwise inclination angle of $z_{\mathrm{spine}}$ [Fig. 2(b)]. Here, we plot the positive helical angle range because of the symmetry with respect to $0^\circ$ [40]. Thus, the helical angle of the identified structures is distributed over a wide range, but this range depends on the meandering magnitudes. As seen, the large helical angle ($>10^\circ$) is observed for the mild meandering structures ($0.05 \leqslant \xi_2/\delta < 0.2$), whereas the range of the distribution becomes narrow beyond $\xi_2 > 0.2$ (i.e., strong meandering structures). Interestingly, the mean helical angle is approximately constant ($\approx 4.3^\circ$) regardless of $\xi_2$, indicating that the wall-attached $u$ structures are statistically aligned along $\pm 4^\circ$ with respect to the streamwise direction. This result is consistent with the previous works [40,44], which reported that long $u$ structures are principally aligned along the helical angles of $4^\circ$–$8^\circ$ in turbulent pipe flows. It is worth noting that the helical angle shown in the present work is obtained from the projection area of three-dimensional structures. In contrast, the aforementioned works computed the helical angles based on the $x$-$z$ plane in the logarithmic region. Moreover, we demonstrate the constant mean helical angle of the identified structures irrespective of their meandering behavior. This observation supports the conjecture that wall-attached $u$ structures statistically maintain their spanwise inclination angle when they undergo the meandering motion.

It is worth mentioning that the results shown in Fig. 4 can be used to improve the attached-eddy model (AEM) proposed by Refs. [57] and [58]. Recently, Ref. [44] found that the synthetic flow fields generated through the AEM well represent the spatial organization of large-scale structures when the AEM is aligned along their helical angles (i.e., the spanwise inclination angle with respect to the flow direction) identified from the proper orthogonal analysis. In addition, Ref. [45] also modified the AEM by considering the additional parameter related to the helical angles. Although these previous works showed refinements to the AEM, they obtained the helical angle from the wall-parallel plane. Given that the AEM [58] was conceived as a three-dimensional model based on the hairpin packet concept [10], the relationship between the helical angle and the lengthscales of three-dimensional structures is required for the AEM to reflect the spatial organization of the coherent structures. In this regard, it would be instructive to refine the AEM in future efforts by imposing scale-specific information for the spatial organization of three-dimensional structures.

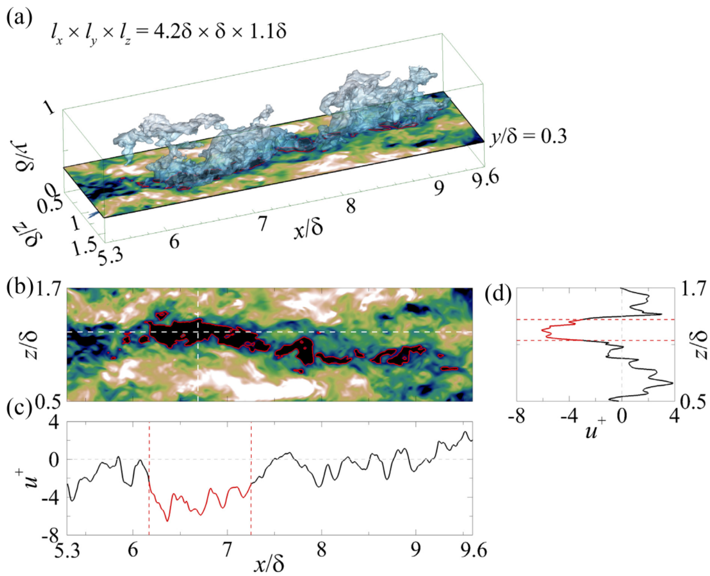


FIG. 5. (a) A sample wall-attached structure in Fig. 2. (b) Contours of instantaneous $u$ in the $x-z$ plane at $y/\delta = 0.3$. The contour levels are the same as in Fig. 1(b). The red line denotes a slice of the identified object in (a). (c,d) Variations of the $u$ signal at $z/\delta = 1.2$ and $x/\delta = 6.7$, indicated by the horizontal and vertical dashed lines in (b), respectively. Here, the red solid lines represent $u$ within the identified structure.

### B. Conditional velocity correlations

The helical angles of coherent structures in the logarithmic region are attributed to a distinct pattern in the two-point correlation of $u$. Given that the long meandering motions are positively and negatively aligned along the streamwise direction, this behavior contributes to the presence of an X-shaped pattern in the two-point correlation as reported previously [13,40,44]. In other words, this distinct feature is a consequence of the superposition of positive and negative alignment of streaky $u$ regions in the logarithmic region. In this section, we will demonstrate this behavior through the conditional two-point correlation by focusing on the streamwise velocity fluctuations carried by positively or negatively aligned structures.

We conditionally sample the streamwise velocity fluctuations contained within the wall-attached structures and label those signals according to the structures' spatial characteristics (i.e., their sizes and meandering magnitude). Figure 5(a) shows a sample $u$ structure, and the wall-parallel slice at $y/\delta = 0.3$ is illustrated in Fig. 5(b). We extract the streamwise velocity fluctuations within the bounded area of each structure, denoted by the red solid line in Fig. 5(b). Figures 5(c) and 5(d) shows the raw $u$ signals along the streamwise and spanwise directions, respectively. Here, the red solid line denotes the streamwise velocity fluctuations contained within the identified structure. As a result, the extracted signals can be labeled according to $\xi_2$ at a given wall-normal location. We could conditionally sample the streamwise velocity fluctuations associated with the meandering motions by applying this procedure to all of the identified structures in the entire flow field. The streamwise velocity fluctuations associated with the identified structures ($u_I$) for a given $\xi_2$ range with the helical angle are conditionally sampled from the entire flow field ($u$) based on the volume of each cluster,

$$u_I(\mathbf{x}) = \begin{cases} u(\mathbf{x}) & \text{if } \mathbf{x} \in \Omega_I, \\ 0 & \text{otherwise,} \end{cases} \tag{2}$$

where $\mathbf{x}$ denotes the position $\mathbf{x} = (x, y, z)$ and $\Omega_I$ indicates all of the positions contained within the identified structure in a given instantaneous flow field; e.g., $\Omega_I$ of the wall-attached structures corresponds to all of the grid points within the isosurfaces shown in Fig. 1(a). In other words, the domain size of the filtered flow field ($u_I$) is consistent with that of the unfiltered flow field ($u$). Although the fluctuating signals outside of the conditionally sampled structures are zero-padded, $u$ changes rapidly near the structures' edges [indicated by red dashed lines in Figs. 5(c) and 5(d)]. This indicates that $u_I$ can retain the spectral characteristics of raw $u$ signals even if we artificially impose zero velocity outside of the identified structures [55]. Reference [59] also reported that the binary representation of conditionally sampled negative-$u$ signals could preserve the spectral information of raw $u$ because of the large changes in $u$ at the edges of the identified structures.

The conditional two-point correlation is defined as

$$R_{u_I u_I}(r_x, y, r_z; y_{\text{ref}}) = \frac{\langle u_I(x, y_{\text{ref}}, z) u_I(x + r_x, y_{\text{ref}}, z + r_z)\rangle}{\langle u_I(x, y_{\text{ref}}, z) u_I(x, y_{\text{ref}}, z)\rangle}, \tag{3}$$

where $u_I$ indicates the streamwise velocity fluctuations within the identified structures at a given $\xi_2$ range and helical angle. The present two-point correlation reflects the streamwise velocity fields associated with the specific events and thus reveals the statistical structure of wall-attached meandering $u$ structures. As discussed in Sec. III A, $u_I$ can be classified into weak meandering structures ($\xi_2/\delta < 0.05$), mild meandering structures ($0.05 \leqslant \xi_2/\delta < 0.2$), and strong meandering structures ($\xi_2/\delta \geqslant 0.2$). Hence, the corresponding conditionally sampled $u$ are $u_{wm}$, $u_{mm}$, and $u_{sm}$, respectively. The event $u_I$ is further conditioned according to the sign of the helical angle. The present conditional correlation Eq. (3) is similar to the expression by Refs. [60,61], who studied the conditional two-point correlations for positive and negative $u$ regions. Similarly, we can conditionally sample $v$ or $w$ within the specific instantaneous structures.

Figure 6 shows the conditional two-point correlations in the wall-parallel planes. Here, we choose two wall-normal locations located at the logarithmic region ($y^+_{\text{ref}} = 110$) and the outer region ($0.3\delta^+$). The red and blue contour lines represent the conditional correlation for positive and negative helical angles. At $y^+_{\text{ref}} = 110$ [Figs. 6(a), 6(c) and 6(e)], it is evident that the red or blue contour lines are aligned along a specific positive or negative angle, respectively, relative to the streamwise direction. This result directly supports the idea that the X-shaped correlation observed in the logarithmic region [13] is a consequence of long meandering $u$ structures with helical angles [40]. More importantly, the contours are aligned along a similar helical angle of 4°, indicated by solid lines, regardless of the meandering magnitude [Figs. 6(a), 6(c) and 6(e)]. The helical angle that appears in the conditional correlation is an imprint of the dominant helical angle for wall-attached $u$ structures; this is also consistent with the mean helical angle obtained in Fig. 4(d). The streamwise or spanwise extensions of the conditional correlation for the weak meandering structures [Fig. 6(e)] are significantly shorter than the other cases [Figs. 6(a) and 6(c)]. However, these conditional correlations exhibit a similar X pattern. In particular, the streamwise extension of the lowest contour levels is approximately $6\delta$ for the strong or mild meandering structures [Figs. 6(a) and 6(c)], whereas those for the weak meandering one is less than $3\delta$ [Fig. 6(e)]; the former is associated with very-large-scale motions, while the latter is related to large-scale motions. This result may, at least statistically, support the conjecture that the concatenation of large-scale motions can be attributed to the formation of very-large-scale motions [16,24,40,44,62]. However, analysis of the evolution of wall-attached $u$ structures with focus on the helical angle when the merging event occurs between the upstream and downstream structures is required for confirmation in this regard.

In the mild and strong meandering cases, we can observe the X-shaped correlations at the outer region. This pattern is very similar to those observed in the logarithmic region [compare Figs. 6(b) and 6(d) with Figs. 6(a) and 6(c), respectively]. It is worth highlighting that the X-like pattern is observed in the two-point correlation of the total $u$ in the outer region [45,61]. This reflects that the wall-attached $u$ structures with $\xi_2 > 0.05\delta$ extend above the logarithmic region and meander substantially even in the outer region ($y/\delta > 0.2$–$0.3$). For the weak meandering case [Fig. 6(f)], on the other hand, the inclination angle is much larger than the helical angles of 4°, and the

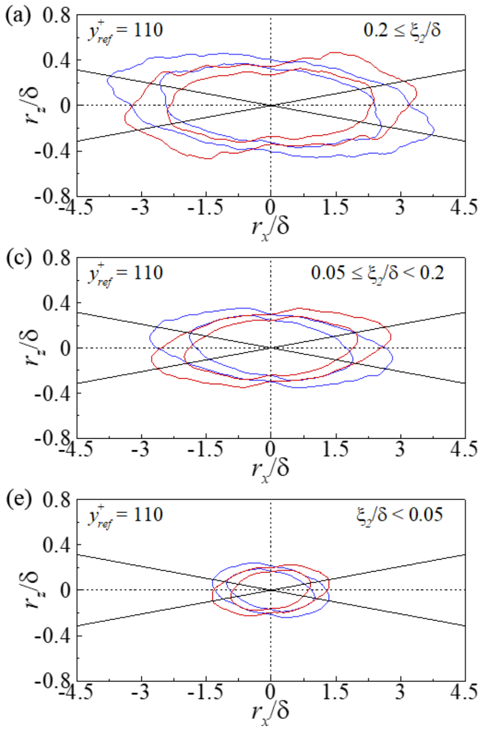


FIG. 6. Conditional two-point correlations in the $x$-$z$ plane ($y = y_{\mathrm{ref}}$): (a,b) $0.2 \leqslant \xi_2/\delta$; (c,d) $0.05 \leqslant \xi_2/\delta < 0.2$; and (e,f) $\xi_2 < 0.05$. The blue and red lines represent the positive and negative helical angles, respectively. The contour levels correspond to 0.02 and 0.04. The straight solid lines indicate the mean helical angle of $\pm 4^{\circ}$.

streamwise lengthscale is decreased compared to the correlation at $y^+_{\mathrm{ref}} = 110$ [Fig. 6(e)]. This behavior is consistent with the wall-normal variation of the conditional correlation of large-scale motions obtained through a spectral filter [44], representing that the weak meandering group mainly consists of the wall-attached $u$ structures with the mean streamwise length of 1–2$\delta$ [see Fig. 4(c)].

To further explore the conditional two-point correlation, we plot the cross-stream plane in Fig. 7. Here, we only plot the negative helical angle case because the positive helical angle case is opposite with respect to $r_z = 0$. For comparison, we plot the two-point correlation of $u$ ($R_{uu}$). At $r_x/\delta = 0$, the two-point correlations are symmetrical with respect to $r_z = 0$ regardless of the $\xi_2$ range. However,

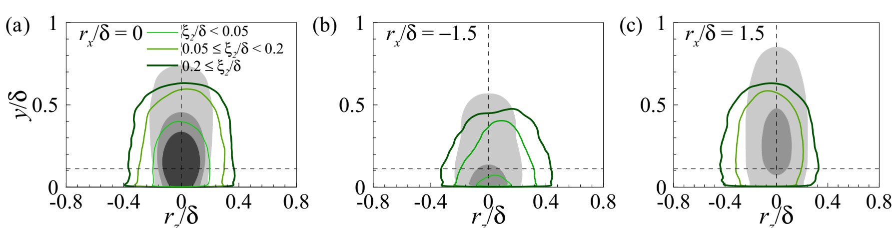


FIG. 7. Conditional two-point correlations in the $y$-$z$ plane for (a) $r_x/\delta = 0$, (b) $r_x/\delta = -1.5$, and (c) $r_x/\delta = 1.5$. Here, we plot the negative helical angle case corresponding to the blue contours in Fig. 6. The horizontal dashed line indicates the reference wall-normal location $y^+_{\mathrm{ref}} = 110$. The line contour level corresponds to 0.02 and its color represents the conditional correlations for the different range $\xi_2$. The shaded contours are $R_{uu} = 0.02$, 0.1, and 0.2.

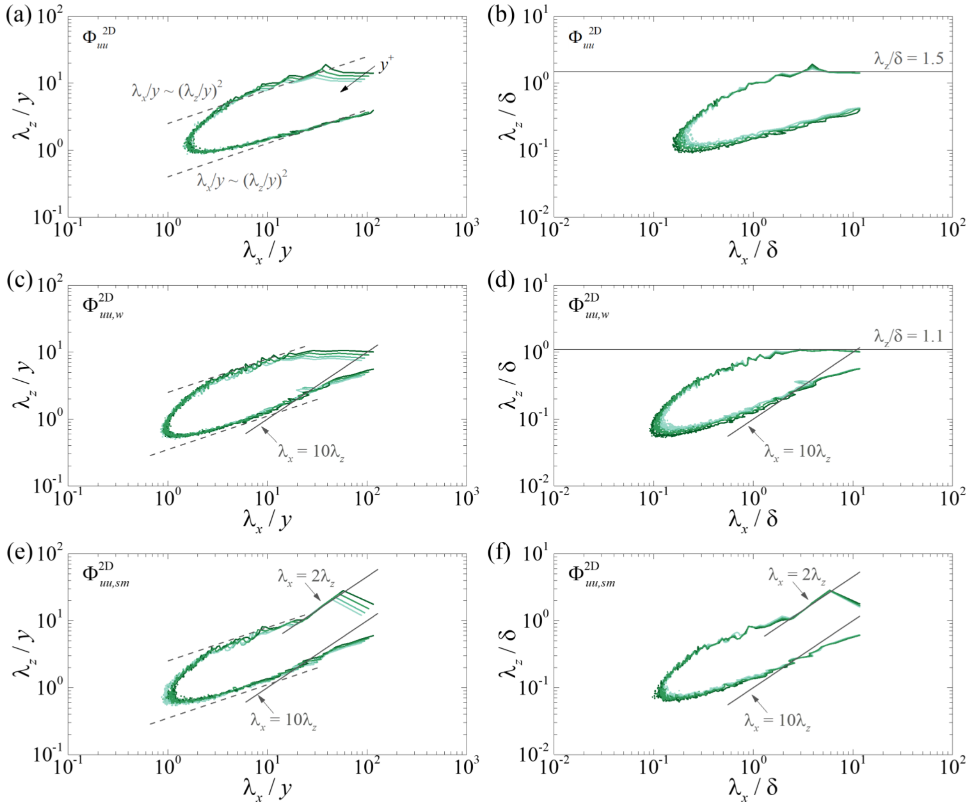


FIG. 8. Premultiplied two-dimensional energy spectra across the logarithmic region ($y^+ = 100$, 110, 120, and 130): (a,b) $\Phi_{uu}^{2D}$; (c,d) $\Phi_{uu,w}^{2D}$; and (e,f) $\Phi_{uu,sm}^{2D}$. The contour level corresponds to 0.4 times each of the maxima. Light to dark shading denotes an increase in the wall-normal distance. The energy spectra are plotted as a function of the wall-parallel wavelengths normalized by $y$ (a,c,e) and $\delta$ (b,d,f). The dashed and solid lines indicate $\lambda_x/y \sim (\lambda_z/y)^2$ and $\lambda_x \sim \lambda_z$, respectively. In (b,d), the horizontal lines denote $\lambda_z/\delta = 1.5$ and 1.1.

the conditional correlations are asymmetric at $r_x/\delta = -1.5$ and 1.5—e.g., the centroid of each line contour is located at $r_z > 0$ [Fig. 7(b)] and $r_z < 0$ [Fig. 7(c)]. This result indicates that the identified structures are statistically tilted across the flow. In addition, the two-point correlations for the mild and strong meandering cases exhibit larger spanwise extents, as compared to $R_{uu}$, at all of the cross-stream planes, implying that the wall-attached $u$ structures with $\xi_2/\delta > 0.02$ comprise a longer and wider range of scales. However, the conditional correlation shown in this section is a consequence of a wide range of different scales. Thus, it is necessary to examine the spectral contribution of turbulence motions according to the meandering magnitude. The following section discusses the two-dimensional energy spectra in the logarithmic region to elucidate the relationship between the X pattern observed in the conditional correlation and the energy distribution across the wall-parallel wavelengths especially in large-scale ranges.

### C. Two-dimensional energy spectra

The spectral contribution of turbulence scales to the streamwise variance is explored by computing the premultiplied two-dimensional energy spectrum of the streamwise velocity. Figures 8(a) and 8(b) show the contours of the premultiplied two-dimensional spectrum of the streamwise velocity $\Phi_{uu}^{2D}$ that is expressed as

$$\Phi_{uu}^{2D}(k_x, k_z, y) = k_x k_z \langle \hat{u}(k_x, k_z, y)\hat{u}^*(k_x, k_z, y)\rangle, \tag{4}$$

where $k_x$ ($= 2\pi/\lambda_x$) and $k_z$ ($= 2\pi/\lambda_z$) are the streamwise and spanwise wave numbers, and $\hat{u}$ and $\hat{u}^*$ denote the Fourier coefficient of $u$ and its complex conjugate. Here, the wall-normal distances correspond to $y^+ = 100$, 110, 120, and 130 located in the logarithmic region. Notably we focus on the lower and upper bounds of the two-dimensional spectra by following Refs. [19,63,64] to examine the energy distribution over the large-scale range, in light of Townsend's attached-eddy hypothesis. In particular, Ref. [63] modeled the two-dimensional spectra based on the attached-eddy hypothesis, in which the energy contributed from the attached eddies is $O(u_\tau^2)$ over the spectral range $\lambda \sim O(y)$ [19,65]. Given the self-similarity of the attached eddies, this spectral region should be bounded by the linear relationship $\lambda_x \sim \lambda_z$ [64]. In this respect, we analyze the slopes of the two-dimensional spectra isocontours, which can serve as the spectral signatures of self-similar motions.

In the large-scale range ($\lambda_x/y > 10$), we can observe that the contours are bounded by the two parallel dashed lines, which represent the square-root relationship $\lambda_x/y \sim (\lambda_z/y)^2$ in Fig. 8(a). This spectral behavior is consistent with the result of Ref. [19] in turbulent channel flow. In addition, at very large streamwise wavelength $\lambda_x/\delta > 3$, the spanwise wavelength of $\Phi_{uu}^{2D}$ is bounded by $\lambda_z/\delta \approx 1.5$ [horizontal line in Fig. 8(b)]. The confinement of the spanwise wavelength with an order of $\delta$ reflects that the spanwise growth of very-large-scale coherent motions is saturated as they close to the edge of the boundary layer [19,50]. This argument is also supported by the work of Ref. [46], which showed that the mean width of wall-attached $u$ structures linearly increases with the structures' height ($l_y$), but the mean width becomes constant as $l_y$ approaches $\delta$. As shown in Fig. 8(b), the upper bound of $\Phi_{uu}^{2D}$ is $\lambda_z/\delta \approx 1.5$, which is slightly lower than $\lambda_z/\delta \approx 2$–3 found in turbulent channel flow [19]. This difference might be due to the entrainment of nonturbulent fluid into the outer layers of TBL.

It is worth noting here that there is no evidence of the existence of self-similar motions in the energy spectrum of the total $u$ because the linear relationship (i.e., $\lambda_x/y \sim \lambda_z/y$) is absent in the large-scale range ($\lambda_x/y > 10$). The linear behavior in the energy spectrum was found in Refs. [64,66] at high-Reynolds-number TBL ($\mathrm{Re}_\tau \approx 2 \times 10^4$). Recently, Ref. [55] decomposed wall-attached $u$ structures into self-similar and non-self-similar objects based on their physical sizes; self-similar structures have their heights over $3\,\mathrm{Re}_\tau^{1/2} < l_y^+ < 0.6\delta^+$ and their mean $l_x$ and $l_z$ are characterized by $l_y$, whereas non-self-similar ones have the heights $l_y \geqslant 0.6\delta$ and the mean $l_x$ is greater than $\delta$. They showed the linear behavior ($\lambda_x \approx 10\lambda_z$) of the lower bound of the two-dimensional spectra at a moderate Reynolds number ($\mathrm{Re}_\tau \approx 1000$) by extracting $u$ signals within wall-attached self-similar structures according to $l_y$. We can see a similar linear relationship in Figs. 8(c) and 8(d), which demonstrates the premultiplied two-dimensional spectra of the streamwise velocity within the wall-attached $u$ structures $\Phi_{uu,w}^{2D}$. As introduced in Fig. 5, we conditionally sample the streamwise velocity based on the bounded volume of the identified structures. In other words, in contrast to the work of Ref. [55], $\Phi_{uu,w}^{2D}$ not only includes the contributions from $u$ of wall-attached self-similar structures but also consists of $u$ of wall-attached non-self-similar structures. However, the lower bounds of $\Phi_{uu,w}^{2D}$ are roughly aligned along $\lambda_x \approx 10\lambda_z$ in both $y$ and $\delta$ scaling [Figs. 8(c) and 8(d)] over 10–20$y < \lambda_x < 3\delta$. This spectral behavior indicates that although the physical sizes (i.e., $l_x$ and $l_z$) of wall-attached non-self-similar structures are characterized by $\delta$, these structures include the self-similar turbulence scales (i.e., $\lambda_x \approx 10\lambda_z$) among a wide range of scales. It also supports the concept of nested hierarchies that larger wall-attached $u$ structures could possess several smaller objects in physical space. For example, one large wall-attached $u$ structure is split into several small $u$ structures when we increase the threshold or the isosurface level; see further discussion provided by Refs. [46,51]. Thus, we could observe the linear relationship in Figs. 8(c) and 8(d); even the spectral contribution of $u$ within wall-attached non-self-similar structures is included in $\Phi_{uu,w}^{2D}$.

For the upper bound of $\Phi^{2D}_{uu,w}$ in Fig. 8(d), the contour lines are aligned along the horizontal line of $\lambda_z/\delta = 1.1$, indicating that the spanwise scales of large motions are restricted, similar to those observed in Fig. 8(b). However, the upper bound of $\Phi^{2D}_{uu,w}$ ($\lambda_z/\delta = 1.1$) is slightly smaller than that of $\Phi^{2D}_{uu}$ ($\lambda_z/\delta = 1.5$). Given that $\Phi^{2D}_{uu,w}$ represents the spectral distribution of coherent motions within wall-attached $u$ structures, such a difference implies the existence of wall-detached large-scale motions. In other words, the decrease of the largest spanwise wavelength in Fig. 8(d) is due to the absence of the spectral contribution of $u$ within wall-detached structures with a large spanwise width. This conjecture is further supported by Ref. [49], which showed the existence of wall-detached $u$ structures with $l_z \sim O(\delta)$ in the outer region. In addition, Ref. [67] reported the spectral contribution of wall-detached (or wall-incoherent) large scales in the energy spectrum.

It is important to note that Townsend's attached-eddy hypothesis requires the linear relationship for both the upper and lower bounds of the two-dimensional energy spectra in the large-scale range in order to assure self-similarity. As discussed above, the upper bound of $\Phi^{2D}_{uu,w}$ does not follow the linear relationship [Fig. 8(c)]. Such spectral behavior was observed at high $\mathrm{Re}_\tau$ flows [64,66]. At low $\mathrm{Re}_\tau$ ($\approx$1000), Ref. [55] showed the linear behavior of the upper bound in the large-scale range by extracting wall-attached self-similar structures in instantaneous flow fields, but the range was very narrow due to a low Reynolds number, i.e., the restriction of the spanwise growth of wall-attached $u$ structures.

To explore the spectral behavior of $u$ contained within the strong meandering motion, the premultiplied energy spectra of $u_{sm}$ ($\Phi^{2D}_{uu,sm}$) are examined. Here, $\Phi^{2D}_{uu,sm}$ is defined as

$$\Phi^{2D}_{uu,sm}(k_x, k_z, y) = k_x k_z \langle \hat{u}_{sm}(k_x, k_z, y)\hat{u}^*_{sm}(k_x, k_z, y)\rangle, \tag{5}$$

where $\hat{u}_{sm}$ denotes the Fourier coefficient of $u_{sm}$ and the asterisk indicates the complex conjugate. In other words, a two-dimensional Fourier transformation of the conditional correlation in Figs. 6(a) and 6(b) corresponds to the two-dimensional spectrum of $u_{sm}$ at a given wall-normal distance,

$$\langle \hat{u}_{sm}(k_x, k_z, y)\hat{u}^*_{sm}(k_x, k_z, y)\rangle = \iint R_{u_{sm}u_{sm}}(r_x, r_z, y)e^{-j2\pi(k_x r_x + k_z r_z)} dr_x dr_y. \tag{6}$$

Interestingly, we can observe a clear linear relationship ($\lambda_x = 2\lambda_z$) in the premultiplied energy spectra of $u$ within the strong meandering wall-attached structures ($\Phi^{2D}_{uu,sm}$) in Figs. 8(e) and 8(f). In addition, the upper bound of $\Phi^{2D}_{uu,sm}$ scales well with both $y$ and $\delta$ over a similar wavelength range. This observation supports the spectral overlap argument of self-similar motions [68]. In particular, the linear relationship appears over a broad range $10y < \lambda_z < 3\delta$ [Fig. 8(f)], indicating that the meandering motions can carry the energy at large spanwise scales $\lambda_z > \delta$. Furthermore, the transition of the upper bound from the square-root behavior to the linear behavior occurs at $\lambda_z \approx 10y$. This transition location is approximately similar to Ref. [64], which found the onset of the linear relationship at $\lambda_z > 10y$ in the two-dimensional spectra of the total $u$ through the high-Re TBL experiment ($\mathrm{Re}_\tau \approx 26\,000$).

Due to the low $\mathrm{Re}_\tau$ of the present TBL data, there is insufficient space to preserve self-similar motions with large spanwise scales ($\lambda_z > \delta$) in the logarithmic region. However, the present result shows that there exist self-similar motions with a lower aspect ratio ($\lambda_x/\lambda_z \approx 2$) if we properly extract these motions, which are contained within wall-attached meandering $u$ structures. To further support this argument, we examine the premultiplied two-dimensional energy spectra according to the meandering magnitudes ($\xi_2$). Figure 9 demonstrates the energy spectra of $u$ contained within the weak meandering, mild meandering, and strong meandering structures ($\Phi^{2D}_{uu,wm}$, $\Phi^{2D}_{uu,mm}$, and $\Phi^{2D}_{uu,sm}$). We plot the energy spectra at two wall-normal locations $y^+ = 100$ and 150, corresponding to the lower and upper limits of the logarithmic region, respectively. Here, the light to dark shading denotes an increase in $\xi_2$. Evidently, all the contours collapse well over $\lambda_x/y < 10$–20 regardless of the meandering magnitudes, but the contours of $\Phi^{2D}_{uu,wm}$ differ from the others. Interestingly, the contour lines in the upper right-hand corner are more inclined to the $\lambda_z$ direction with increasing the meandering magnitudes. Reference [13] observed similar behavior in the two-dimensional spectra

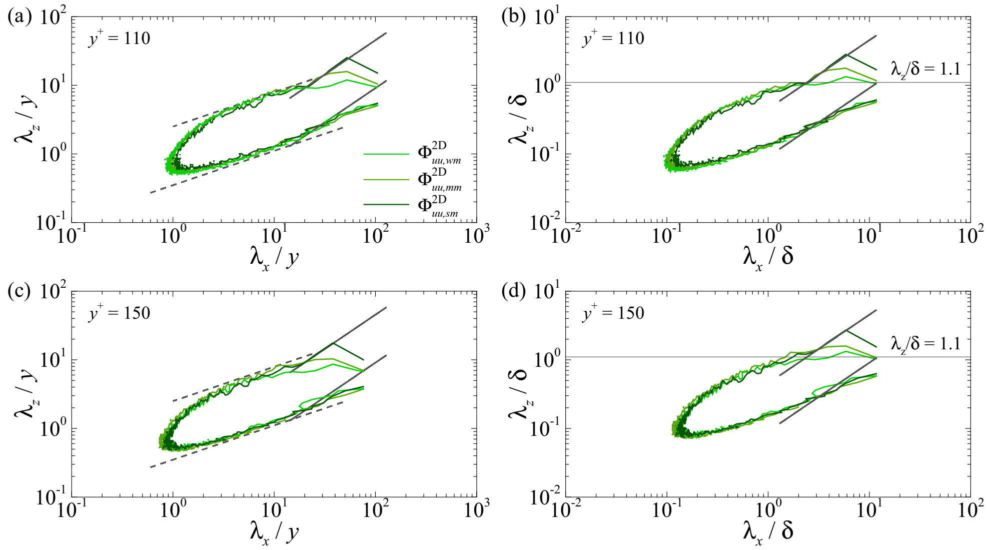


FIG. 9. Premultiplied two-dimensional energy spectra at $y^+ = 110$ (a,b) and 150 (c,d). The contour level corresponds to 0.4 times each of the maxima. The energy spectra are plotted as a function of the wall-parallel wavelengths normalized by $y$ (a,c) and $\delta$ (b,d). The dashed and solid lines correspond to those in Fig. 8.

of synthetic sinusoidal $u$ signals. Still, there was no linear relationship between $\lambda_x$ and $\lambda_z$ since $u$ signals were synthesized based on sinusoidal functions.

It is evident that $\Phi^{2D}_{uu,wm}$ (light green contour) is consistent with $\Phi^{2D}_{uu,w}$ in Figs. 8(c) and 8(d), which is the energy spectra of $u$ within wall-attached $u$ structures. For $\Phi^{2D}_{uu,wm}$, there is no linear behavior of the upper bound, rather the energy distribution of the large spanwise scale is restricted by $\lambda_z/\delta = 1.1$ in an analogous manner to that for $\Phi^{2D}_{uu,w}$. Given that most of the wall-attached structures exhibit the meandering magnitude less than 0.5 (see Fig. 4), $\Phi^{2D}_{uu,wm}$ resembles $\Phi^{2D}_{uu,w}$, which in turn contributes to the absence of $\lambda_x \approx 2\lambda_z$ behavior in $\Phi^{2D}_{uu,wm}$ over the large-scale range.

On the other hand, the linear relationship $\lambda_x \approx 2\lambda_z$ is observed for $\Phi^{2D}_{uu,sm}$ (dark green contour), which indicates that to assure the $\lambda_x \approx 2\lambda_z$ behavior, $\xi_2$ should be at least greater than $0.05\delta$. As discussed above, the spanwise scales of wall-attached structures need to be larger than $\delta$ for the presence of this behavior at the present Reynolds number. In Sec. III A, we find that the width of the weak meandering structures is less than $\delta$ [see Fig. 4(b)], whereas that of the mild meandering or strong meandering groups includes the structures with $l_z > \delta$. Therefore, the present results demonstrate that the spanwise growth of energy-containing motions in the logarithmic region can be saturated as their heights approach $\delta$, but the strong meandering structures (e.g., $\xi_2 > 0.2\delta$) have a large spanwise scale compared to their streamwise scale. Moreover, these severely meandering structures contribute to the linear spectral behavior, which is the requirement for self-similarity predicted by the attached-eddy hypothesis.

It is worth highlighting that the structural-based turbulence model based on Townsend's hypothesis is a conceptual model that describes the kinematics of wall turbulence in terms of representative eddies in the logarithmic region [54]; that is, these eddies are considered statistical structures that represent the gross features of an assemblage of eddies at a different stretching stage [42,57]. Furthermore, Townsend's hypothesis assumes inviscid flows with an asymptotically high Reynolds number. As a result, this model cannot fully explain the dynamics of the (large-scale) coherent structures that occur in real turbulent flows. To overcome these limitations, it is necessary to examine their dynamics and interactions with other scales, which can provide us with the information needed to improve the attached-eddy model and develop a new flow control strategy. Given that attached

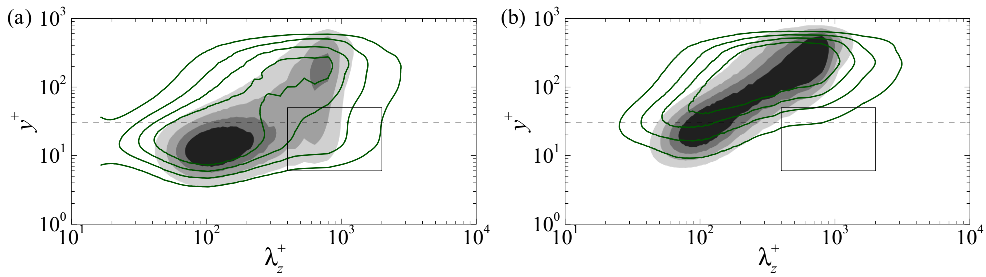


FIG. 10. Premultiplied one-dimensional spanwise energy spectra: (a) $\Phi_{uu}^{1D}$ (shaded contour) and $\Phi_{uu,w}^{1D}$ (line contour); and (b) $\Phi_{uv}^{1D}$ (shaded contour) and $\Phi_{uv,w}^{1D}$ (line contour). The contour levels are 0.25, 0.4, 0.55, and 0.7 times of each maximum. The near-wall part of large scales is highlighted with an inserted box. The horizontal dashed line denotes $y^+ = 30$.

eddies in the logarithmic region sustain themselves similarly to the self-sustaining cycle of near-wall coherent structures [69], it would be interesting in future efforts to explore the dynamic behavior of the meandering motions of wall-attached structures and the surrounding vortical structures simultaneously. Since very long $u$ structures experience a rapid sinuous meandering motion and regenerate vortical structures [69,70], the meandering magnitudes could be an indicator representing a stage of sustaining cycle of wall-attached structures.

### D. Footprints of meandering motions

In this section, we further discuss the near-wall part (i.e., footprint) of the large-scale meandering structures, which is essentially associated with the "inactive" component of the attached eddies [41]. Townsend [41] described attached eddies as active and inactive motions depending on whether such eddies are responsible for generating the Reynolds shear stress. Due to the wall's impermeable boundary condition, the near-wall part of attached eddies (i.e., $y/l_y \approx 0$, where $l_y$ is the height of attached eddies) is blocked by the wall, which leads to $v \approx 0$ and nonzero values for the wall-parallel velocity components. In other words, all attached eddies can be active over the region where the wall-normal distance is close to the center of attached eddies ($y_c \approx l_y/2$), whereas large and tall attached eddies can have an inactive part close to the wall (e.g., $y < y_c$) if it contributes to the Reynolds shear stress smaller than other scales [65,71,72]. Given that the meandering motions of long $u$ structures are responsible for the generation of $v$ through the breakdown of the meandering motions [69], one could conjecture that the strong meandering structures, whose mean heights are an order of $\delta$, that were identified in the present work contain relatively intense $v$ in the outer region. In addition, Ref. [39] noted that the meandering motions of superstructures in the outer region extend down to the wall, which leads to a strong streamwise gradient of $u$ in the near-wall region. This implies that the footprint of strong meandering structures also meanders in the near-wall region and that such footprints can contribute to the momentum transfer. Therefore, we further analyze the turbulent motions contained within the near-wall part of strong meandering structures by focusing on the energy spectra of the streamwise velocity fluctuations and the Reynolds shear stress in the near-wall region.

The gray contours in Figs. 10(a) and 10(b) show the premultiplied one-dimensional spanwise spectra of $u$ and $uv$ ($\Phi_{uu}^{1D}$ and $\Phi_{uv}^{1D}$). The inserted box denotes the region of interest, where $y^+ < 50$ and $\lambda_z^+ > 0.4$–$0.5\delta^+$. In Fig. 10(a), we can decompose the spectral domain into small- and large-scale ranges with the cutoff wavelength $\lambda_z^+ = 0.4$–$0.5\delta^+$ because this value demarcates the inner and outer peaks [32,73]. This is close to the mean spanwise size of large-scale outer structures observed in the two-point correlation of $u$ (see the gray contours in Fig. 7). We can also observe the existence of large scales in the near-wall region, indicating the superimposed large scales of the near-wall footprints [13,27]. Given that these (very) large scales carry a significant amount of the Reynolds shear stress in the outer region [20,21,24], we can describe these motions as active in the outer region where the wall-normal distance is close to their center ($y \approx y_c$), in the view of Townsend [41]. Figure 10(b) expresses the one-dimensional spectrum of the Reynolds shear stress, which shows that the energy contained within the large-scale motions is located in the outer region. On the other hand, the contours of $\Phi_{uv}^{1D}$ do not extend down to the wall, representing that the large scales are relatively inactive in the near-wall region compared to the smaller scales at the same wall-normal distance [27,65,72].

The green contours in Fig. 10 illustrate the one-dimensional spanwise energy spectra for the strong meandering motion. Figure 10(a) presents the spectrum of $u_{sm}$ ($\Phi_{uu,sm}^{1D}$), which was obtained by integrating the two-dimensional energy spectra along the streamwise wavelength, and it shows that the lowest isocontours in the large-scale range extend down to the wall. This feature demonstrates that the superimposed large scales in the near-wall region were similar to those of $\Phi_{uu}^{1D}$ (gray contour) but that the footprint of the meandering structures contained a much wider spanwise wavelength ($\lambda_z \approx 2\delta$). We plot the spectrum of the Reynolds shear stress for the strong meandering motion $\Phi_{uv,sm}^{1D}$ [green contours in Fig. 10(b)] to discern whether the footprint of the strong meandering motion can carry the Reynolds shear stress. As seen, $\Phi_{uv,sm}^{1D}$ extend to wider $\lambda_z$ in the near-wall region (compare with $\Phi_{uv}^{1D}$), representing that the wider wavelengths have energy from the near-wall region to the outer region that is similar to those observed in $\Phi_{uu}^{1D}$. Here, we plot the energy spectra normalized by each maximum in order to examine the relative contribution of turbulent motions within the meandering structures. Hence, the existence of large-scale contribution does not imply that the near-wall large-scales significantly contribute to the total Reynolds shear stress because of the absence of such a contribution in $\Phi_{uv}^{1D}$ contours. However, this result indicates that the footprints of the large-scale meandering motion carry both $u$ and (some) $v$, and they are responsible for some amount of the Reynolds shear stress in the near-wall region ($y^+ < 50$). This spectral range is similar to the positive turbulent transport found in Ref. [74], which examined the spanwise spectrum of the turbulent transport and observed a nonzero energy transfer carried by large $\lambda_z$ in the near-wall region. In addition, Ref. [36] observed the migration of near-wall streaks under outer large-scale roll motions that ultimately induce strong ejection events. In this sense, it is conjectured that the near-wall momentum transport over large scales is related to the amplitude modulation of small scales of wall-normal fluctuations [31,32] because of the meandering footprints. Notably, the non-negligible contribution of near-wall large scales in $\Phi_{uv,sm}^{1D}$ does not necessarily indicate that these motions are active in the near-wall region. Rather, they carry a minor amount of the Reynolds shear stress.

Additionally, $\Phi_{uv,sm}^{1D}$ in Fig. 10(b) shows that there is some wall-normal variation of $\Phi_{uv,sm}^{1D}$ in the near-wall region (i.e., the wall-normal gradient of the Reynolds shear stress spectrum $\partial\Phi_{uv,sm}^{1D}/\partial y$, also called the premultiplied net force spectrum) [20,21,75]. In the streamwise mean momentum equation, $-\partial\langle uv\rangle/\partial y$ accelerates or retards the mean flow as the net fictitious force exerted by the Reynolds shear stress [2,20,76]. Therefore, we can imagine that the meandering footprints could locally accelerate or retard the near-wall velocity fields and that this behavior could be associated with the amplitude or frequency modulation of near-wall small scales [29,32,77,78]. Moreover, we can surmise that the large-scale meandering structures tend to be straight along the streamwise direction because the long streaky $u$ structures are amplified and aligned along the streamwise direction as a result of the interaction with $v$ structures [69]. In this manner, the meandering footprints could potentially lead to local acceleration or deceleration effects in the near-wall region. In future efforts, a more in-depth study is needed to observe the interactions between large-scale dynamics and near-wall cycle by focusing on the meandering footprints of large scales.

Finally, it is worth mentioning the recent progress in our understanding of large-scale motions in connection with Townsend's attached-eddy hypothesis [41]. Several recent works attempted to generalize the attached-eddy hypothesis. For example, Ref. [72] tried to link this hypothesis (i.e., actually inviscid theory because it assumes $\mathrm{Re}_\tau \to \infty$) with the mesolayer concept [76,79] by focusing on the inner-scaling nature of the inactive part of large-scale structures. Reference [80] suggested more generalized characteristic scales of attached eddies based on the mean momentum balance in the fully developed channel flow. Reference [67] used stochastic spectral filters for a wide range of $\mathrm{Re}_\tau$ to provide a more general description for the one-dimensional streamwise energy spectra and the streamwise turbulence intensity profile proposed by Refs. [68] and [81]. In addition, Ref. [82] revisited the spectral overlap argument [68,83] and suggested a more general condition for the spectral overlap region in the one-dimensional streamwise energy spectra.

Although the research has led to much progress on large-scale structures during the past decades, researchers still face an open challenge to combine the findings (both kinematics and dynamics of large-scale structures) and explain them in the viewpoint of Townsend's theory. Specifically, these studies cover (i) the superposition of large scales in the near-wall region [13,27], (ii) the associated scaling failure of near-wall turbulence intensities [84,85], (iii) the amplitude and frequency modulations of near-wall small scales [29,77,78], and (iv) the inner-outer interactions (i.e., top-down and bottom-up interactions) between large-scale dynamics and near-wall cycles [36,86]. Although this work does not directly or thoroughly touch upon these topics, we expect that it will provide an important link for future work because the superimposed meandering motions of large-scale structures in the near-wall region are responsible for the inner-outer interactions and associated modulation effects. Hence, this topic remains an essential theme for future work.

## IV. CONCLUSIONS

We have investigated the influence of meandering motions of wall-attached $u$ structures on the two-point correlation and the premultiplied two-dimensional spectra in the logarithmic region by examining the DNS data of the zero-pressure-gradient TBL at $\mathrm{Re}_\tau \approx 1000$. The meandering motions of three-dimensional $u$ structures that are physically attached to the wall were quantified by extracting the spine from the projected area in the wall-parallel plane. We have shown that the meandering magnitudes $\xi_2$ differ significantly among the identified structure, even when their heights ($l_y$) are similar. This observation reflects that the identified structures are at different stages of sinuous motions. In addition, the minimum length, height, and width of the strong meandering structures ($\xi_2/\delta \geqslant 0.2$) are greater than $\delta$, $0.3\delta$, and $0.5\delta$, respectively, indicating that these strong meandering structures can be considered as large-scale motions or very-large-scale motions that extend across the logarithmic region. Interestingly, the mean spanwise inclination angle was approximately $4.3^\circ$ regardless of $\xi_2$. This result implies that the wall-attached $u$ structures are not only statistically aligned along a certain angle [40,44], but they may maintain their spanwise inclination angle when they undergo the meandering motions.

The conditional two-point correlations for the positive and negative spanwise angles show a distinct X pattern in the logarithmic region. They are aligned with a similar spanwise offset of $4^\circ$, regardless of the meandering magnitudes. This observation directly supports the findings by Ref. [13], which showed the X-shaped correlation through the synthetic sinusoidal $u$ signals that modeled the meandering motions of long $u$ streaks in the logarithmic region.

The premultiplied two-dimensional spectra of the streamwise velocity fluctuations were examined by conditionally sampling the velocity fluctuations contained within the meandering motions $u_{sm}$ to explore how the wall-attached structures' meandering motions influenced the spectral behaviors over the large-scale range ($\lambda_x/y > 10$) in the logarithmic region. The two-dimensional spectra of $u_{sm}$ ($\Phi^{2\mathrm{D}}_{uu,sm}$) show a clear linear relationship $\lambda_x \approx 2\lambda_z$ over a broad range $10y < \lambda_z < 3\delta$, which is absent from the two-dimensional spectra of the total $u$ ($\Phi^{2\mathrm{D}}_{uu}$). In $\Phi^{2\mathrm{D}}_{uu}$, the spanwise scale is bounded by $\lambda_z/\delta \approx 1.5$ at very large streamwise wavelengths of $\lambda_x > \delta$. The confinement of the spanwise wavelength with an order of $\delta$ reflects that the spanwise growth of very large scales becomes saturated as they reach the edge of the flow thickness. The linear relationship observed in $\Phi^{2\mathrm{D}}_{uu,sm}$ indicates that not only does the wall-attached $u$ structure with strong meandering motions ($\xi_2/\delta \geqslant 0.2$) contain the energy at large spanwise scales but the motions also are self-similar. As the meandering magnitudes increase, the contour lines of the spectra become more inclined toward the $\lambda_z$ direction; however, the linear behavior is only observed for the strong meandering structures.

Thus, we demonstrate that the spanwise growth of energy-containing motions in the logarithmic region can be saturated as their heights approach the boundary-layer thickness. This saturation, in turn, contributes to the absence of linear behavior for the upper bound of the two-dimensional spectra at moderate Reynolds numbers. Moreover, the spanwise scales of the spectral energy carried by the tall wall-attached $u$ structures depend on the structures' meandering behaviors. In particular, the strong meandering structures contain self-similar motions reminiscent of Townsend's attached eddies.

To further discuss the near-wall part (i.e., footprint) of the strong meandering structures, which is associated with the "inactive" part of attached eddies [41], we explored the premultiplied one-dimensional spectra of the Reynolds shear stress carried by the meandering structures $\Phi^{1D}_{uu,sm}$. In contrast to $\Phi^{1D}_{uv}$, $\Phi^{1D}_{uv,sm}$ extends to wider $\lambda_z$ in the near-wall region, representing that the wider wavelengths have energy from the near-wall region to the outer region similar to those observed in the one-dimensional spectrum of $u$. This result indicates that the footprints of the large-scale meandering motion carry both $u$ and (some) $v$, and are responsible for some of the Reynolds shear stress in the near-wall region ($y^+ < 50$). In this sense, it is conjectured that the near-wall momentum transport over large scales is related to the amplitude modulation of small scales of wall-normal fluctuations because of the meandering footprints. In future efforts, we expect that examining the dynamics of wall-attached structures and surrounding vortical structures by focusing on the meandering magnitude will facilitate deeper insights into energy transfer via wall-attached structures, leading to developing a new flow control strategy.

## ACKNOWLEDGMENTS

This work was supported by a National Research Foundation of Korea (NRF) grant funded by the Korea government (MSIT) (Grant No. 2020R1F1A1048537) and supported by the Supercomputing Center (KISTI).


[1] S. K. Robinson, Coherent motions in the turbulent boundary layer, Annu. Rev. Fluid Mech. **23**, 601 (1991).

[2] R. J. Adrian, Hairpin vortex organization in wall turbulence, Phys. Fluids **19**, 041301 (2007).

[3] J. Jiménez, Coherent structures in wall-bounded turbulence, J. Fluid Mech. **842**, P1 (2018).

[4] S. J. Kline, W. C. Reynolds, F. A. Schraub, and P. W. Runstadler, The structure of turbulent boundary layers, J. Fluid Mech. **30**, 741 (1967).

[5] J. M. Hamilton, J. Kim, and F. Waleffe, Regeneration mechanisms of near-wall turbulence structures, J. Fluid Mech. **287**, 317 (1995).

[6] J. Jiménez and A. Pinelli, The autonomous cycle of near-wall turbulence, J. Fluid Mech. **389**, 335 (1999).

[7] W. Schoppa and F. Hussain, Coherent structure generation in near-wall turbulence, J. Fluid Mech. **453**, 57 (2002).

[8] L. S. Kovasznay, V. Kibens, and R. F. Blackwelder, Large-scale motion in the intermittent region of a turbulent boundary layer, J. Fluid Mech. **41**, 283 (1970).

[9] R. E. Falco, Coherent motions in the outer region of turbulent boundary layers, Phys. Fluids **20**, S124 (1977).

[10] R. J. Adrian, C. D. Meinhart, and C. D. Tomkins, Vortex organization in the outer region of the turbulent boundary layer, J. Fluid Mech. **422**, 1 (2000).

[11] B. Ganapathisubramani, N. Hutchins, W. Hambleton, E. Longmire, and I. Marusic, Investigation of large-scale coherence in a turbulent boundary layer using two-point correlations, J. Fluid Mech. **524**, 57 (1999).

[12] N. Hutchins, W. T. Hambleton, and I. Marusic, Inclined cross-stream stereo particle image velocimetry measurements in turbulent boundary layers, J. Fluid Mech. **541**, 21 (2005).

[13] N. Hutchins and I. Marusic, Evidence of very long meandering features in the logarithmic region of turbulent boundary layers, J. Fluid Mech. **579**, 1 (2007).

[14] J. Monty, J. Stewart, R. Williams, and M. Chong, Large-scale features in turbulent pipe and channel flows, J. Fluid Mech. **589**, 147 (2007).
[15] J. H. Lee and H. J. Sung, Very-large-scale motions in a turbulent boundary layer, J. Fluid Mech. **673**, 80 (2011).
[16] K. C. Kim and R. J. Adrian, Very large-scale motion in the outer layer, Phys. Fluids **11**, 417 (1999).
[17] J. C. del Álamo and J. Jiménez, Spectra of the very large anisotropic scales in turbulent channels, Phys. Fluids **15**, L41 (2003).
[18] B. Ganapathisubramani, E. K. Longmire, and I. Marusic, Characteristics of vortex packets in turbulent boundary layers, J. Fluid Mech. **478**, 35 (2003).
[19] J. C. del Álamo, J. Jiménez, P. Zandonade, and R. D. Moser, Scaling of the energy spectra of turbulent channels, J. Fluid Mech. **500**, 135 (1999).
[20] M. Guala, S. E. Hommema, and R. J. Adrian, Large-scale and very-large-scale motions in turbulent pipe flow, J. Fluid Mech. **554**, 521 (2006).
[21] B. Balakumar and R. Adrian, Large-and very-large-scale motions in channel and boundary-layer flows, Philos. Trans. R. Soc. A **365**, 665 (2007).
[22] X. Wu, J. R. Baltzer, and R. J. Adrian, Direct numerical simulation of a 30$R$ long turbulent pipe flow at $R^+ = 685$: large- and very large-scale motions, J. Fluid Mech. **698**, 235 (2012).
[23] J. Ahn, J. H. Lee, J. Lee, J.-H. Kang, and H. J. Sung, Direct numerical simulation of a 30$R$ long turbulent pipe flow at $\mathrm{Re}_\tau = 3008$, Phys. Fluids **27**, 065110 (2015).
[24] J. Hwang, J. Lee, and H. J. Sung, Influence of large-scale accelerating motions on turbulent pipe and channel flows, J. Fluid Mech. **804**, 420 (2016).
[25] W.-Y. Zhang, W.-X. Huang, and C.-X. Xu, Very large-scale motions in turbulent flows over streamwise traveling wavy boundaries, Phys. Rev. Fluids **4**, 054601 (2019).
[26] H. Abe, H. Kawamura, and H. Choi, Very large-scale structures and their effects on the wall shear-stress fluctuations in a turbulent channel flow up to re $\tau = 640$, J. Fluids Eng. **126**, 835 (2004).
[27] S. Hoyas and J. Jiménez, Scaling of the velocity fluctuations in turbulent channels up to $Re_\tau = 2003$, Phys. Fluids **18**, 011702 (2006).
[28] N. Hutchins and I. Marusic, Large-scale influences in near-wall turbulence, Philos. Trans. R. Soc. A **365**, 647 (2007).
[29] R. Mathis, N. Hutchins, and I. Marusic, Large-scale amplitude modulation of the small-scale structures in turbulent boundary layers, J. Fluid Mech. **628**, 311 (2009).
[30] L. Agostini and M. A. Leschziner, On the influence of outer large-scale structures on near-wall turbulence in channel flow, Phys. Fluids **26**, 075107 (2014).
[31] K. Talluru, R. Baidya, N. Hutchins, and I. Marusic, Amplitude modulation of all three velocity components in turbulent boundary layers, J. Fluid Mech. **746**, R1 (2014).
[32] J. Hwang and H. J. Sung, Influence of large-scale motions on the frictional drag in a turbulent boundary layer, J. Fluid Mech. **829**, 751 (2017).
[33] I. Marusic, R. Mathis, and N. Hutchins, Predictive model for wall-bounded turbulent flow, Science **329**, 193 (2010).
[34] L. Agostini and M. Leschziner, Predicting the response of small-scale near-wall turbulence to large-scale outer motions, Phys. Fluids **28**, 015107 (2016).
[35] G. Yin, W.-X. Huang, and C.-X. Xu, Prediction of near-wall turbulence using minimal flow unit, J. Fluid Mech. **841**, 654 (2018).
[36] J. Hwang, J. Lee, H. J. Sung, and T. A. Zaki, Inner-outer interactions of large-scale structures in turbulent channel flow, J. Fluid Mech. **790**, 128 (2016).
[37] M. Yoon, J. Ahn, J. Hwang, and H. J. Sung, Contribution of velocity-vorticity correlations to the frictional drag in wall-bounded turbulent flows, Phys. Fluids **28**, 081702 (2016).
[38] M. Yoon, J. Hwang, and H. J. Sung, Contribution of large-scale motions to the skin friction in a moderate adverse pressure gradient turbulent boundary layer, J. Fluid Mech. **848**, 288 (2018).
[39] N. Hutchins, J. P. Monty, B. Ganapathisubramani, H. C. H. Ng, and I. Marusic, Three-dimensional conditional structure of a high-Reynolds-number turbulent boundary layer, J. Fluid Mech. **673**, 255 (2011).

[40] J. R. Baltzer, R. J. Adrian, and X. Wu, Structural organization of large and very large scales in turbulent pipe flow simulation, J. Fluid Mech. **720**, 236 (2013).
[41] A. A. Townsend, *The Structure of Turbulent Shear Flow* (Cambridge University Press, Cambridge, 1976).
[42] A. E. Perry and M. S. Chong, On the mechanism of wall turbulence, J. Fluid Mech. **119**, 173 (1982).
[43] K. Kevin, J. Monty, and N. Hutchins, The meandering behaviour of large-scale structures in turbulent boundary layers, J. Fluid Mech. **865**, R1 (2019).
[44] J. H. Lee, H. J. Sung, and R. J. Adrian, Space–time formation of very-large-scale motions in turbulent pipe flow, J. Fluid Mech. **881**, 1010 (2019).
[45] F. Eich, C. M. de Silva, I. Marusic, and C. J. Kähler, Towards an improved spatial representation of a boundary layer from the attached eddy model, Phys. Rev. Fluids **5**, 034601 (2020).
[46] J. Hwang and H. J. Sung, Wall-attached structures of velocity fluctuations in a turbulent boundary layer, J. Fluid Mech. **856**, 958 (2018).
[47] J. C. del Álamo and J. Jiménez, Linear energy amplification in turbulent channels, J. Fluid Mech. **559**, 205 (2006).
[48] A. Lozano-Durán, O. Flores, and J. Jiménez, The three-dimensional structure of momentum transfer in turbulent channels, J. Fluid Mech. **694**, 100 (2012).
[49] M. Yoon, J. Hwang, J. Yang, and H. J. Sung, Wall-attached structures of streamwise velocity fluctuations in an adverse-pressure-gradient turbulent boundary layer, J. Fluid Mech. **885**, A12 (2020).
[50] J. Han, J. Hwang, M. Yoon, J. Ahn, and H. J. Sung, Azimuthal organization of large-scale motions in a turbulent minimal pipe flow, Phys. Fluids **31**, 041903 (2019).
[51] J. Hwang and H. J. Sung, Wall-attached clusters for the logarithmic velocity law in turbulent pipe flow, Phys. Fluids **31**, 055109 (2019).
[52] J. Yang, J. Hwang, and H. J. Sung, Influence of wall-attached structures on the boundary of the quiescent core region in turbulent pipe flow, Phys. Rev. Fluids **4**, 114606 (2019).
[53] L.-H. Wang, C.-X. Xu, H. J. Sung, and W.-X. Huang, Wall-attached structures over a traveling wavy boundary: Turbulent velocity fluctuations, Phys. Rev. Fluids **6**, 034611 (2021).
[54] I. Marusic and J. P. Monty, Attached eddy model of wall turbulence, Annu. Rev. Fluid Mech. **51**, 49 (2019).
[55] J. Hwang, J. H. Lee, and H. J. Sung, Statistical behaviour of self-similar structures in canonical wall turbulence, J. Fluid Mech. **905**, A6 (2020).
[56] K. Kim, S. J. Baek, and H. J. Sung, An implicit velocity decoupling procedure for the incompressible Navier–Stokes equations, Int. J. Numer. Meth. Fluids **38**, 125 (2002).
[57] A. E. Perry and I. Marusic, A wall-wake model for the turbulence structure of boundary layers. Part 1. Extension of the attached eddy hypothesis, J. Fluid Mech. **298**, 361 (1995).
[58] I. Marusic, On the role of large-scale structures in wall turbulence, Phys. Fluids **13**, 735 (2001).
[59] S. Srinath, J. C. Vassilicos, C. Cuvier, J.-P. Laval, M. Stanislas, and J.-M. Foucaut, Attached flow structure and streamwise energy spectra in a turbulent boundary layer, Phys. Rev. E **97**, 053103 (2018).
[60] J. H. Lee and H. J. Sung, Comparison of very-large-scale motions of turbulent pipe and boundary layer simulations, Phys. Fluids **25**, 045103 (2013).
[61] J. A. Sillero, J. Jiménez, and R. D. Moser, Two-point statistics for turbulent boundary layers and channels at Reynolds numbers up to $\delta^+ = 2000$, Phys. Fluids **26**, 105109 (2014).
[62] J. Lee, J. H. Lee, J.-I. Choi, and H. J. Sung, Spatial organization of large-and very-large-scale motions in a turbulent channel flow, J. Fluid Mech. **749**, 818 (2014).
[63] D. Chung, I. Marusic, J. P. Monty, M. Vallikivi, and A. J. Smits, On the universality of inertial energy in the log layer of turbulent boundary layer and pipe flows, Exp. Fluids **56**, 141 (2015).
[64] D. Chandran, R. Baidya, J. P. Monty, and I. Marusic, Two-dimensional energy spectra in high-Reynolds-number turbulent boundary layers, J. Fluid Mech. **826**, R1 (2017).
[65] J. Jiménez and S. Hoyas, Turbulent fluctuations above the buffer layer of wall-bounded flows, J. Fluid Mech. **611**, 215 (2008).
[66] R. Deshpande, D. Chandran, J. P. Monty, and I. Marusic, Two-dimensional cross-spectrum of the streamwise velocity in turbulent boundary layers, J. Fluid Mech. **890**, R2 (2020).

[67] W. J. Baars and I. Marusic, Data-driven decomposition of the streamwise turbulence kinetic energy in boundary layers. Part 1. Energy spectra, J. Fluid Mech. **882**, A25 (2020).
[68] A. E. Perry, S. Henbest, and M. S. Chong, A theoretical and experimental study of wall turbulence, J. Fluid Mech. **165**, 163 (1986).
[69] Y. Hwang and Y. Bengana, Self-sustaining process of minimal attached eddies in turbulent channel flow, J. Fluid Mech. **795**, 708 (2016).
[70] O. Flores and J. Jiménez, Hierarchy of minimal flow units in the logarithmic layer, Phys. Fluids **22**, 071704 (2010).
[71] Y. Hwang, Statistical structure of self-sustaining attached eddies in turbulent channel flow, J. Fluid Mech. **767**, 254 (2015).
[72] Y. Hwang, Mesolayer of attached eddies in turbulent channel flow, Phys. Rev. Fluids **1**, 064401 (2016).
[73] M. Bernardini and S. Pirozzoli, Inner/outer layer interactions in turbulent boundary layers: a refined measure for the large-scale amplitude modulation mechanism, Phys. Fluids **23**, 061701 (2011).
[74] M. Cho, Y. Hwang, and H. Choi, Scale interactions and spectral energy transfer in turbulent channel flow, J. Fluid Mech. **854**, 474 (2018).
[75] C. Chin, J. Philip, J. Klewicki, A. Ooi, and I. Marusic, Reynolds-number-dependent turbulent inertia and onset of log region in pipe flows, J. Fluid Mech. **757**, 747 (2014).
[76] T. Wei, P. Fife, J. Klewicki, and P. McMurtry, Properties of the mean momentum balance in turbulent boundary layer, pipe and channel flows, J. Fluid Mech. **522**, 303 (2005).
[77] B. Ganapathisubramani, N. Hutchins, J. P. Monty, D. Chung, and I. Marusic, Amplitude and frequency modulation in wall turbulence, J. Fluid Mech. **712**, 61 (2012).
[78] W. Baars, K. Talluru, N. Hutchins, and I. Marusic, Wavelet analysis of wall turbulence to study large-scale modulation of small scales, Exp. Fluids **56**, 188 (2015).
[79] N. Afzal, Fully developed turbulent flow in a pipe: an intermediate layer, Ing.-Arch. **52**, 355 (1982).
[80] A. Lozano-Durán and H. J. Bae, Characteristic scales of Townsend's wall-attached eddies, J. Fluid Mech. **868**, 698 (2019).
[81] I. Marusic and G. J. Kunkel, Streamwise turbulence intensity formulation for flat-plate boundary layers, Phys. Fluids **15**, 2461 (2003).
[82] Y. Hwang, N. Hutchins, and I. Marusic, The logarithmic variance of streamwise velocity and conundrum in wall turbulence, J. Fluid Mech. **933**, A8 (2022).
[83] A. E. Perry and C. J. Abell, Asymptotic similarity of turbulence structures in smooth-and rough-walled pipes, J. Fluid Mech. **79**, 785 (1977).
[84] D. B. De Graaff and J. K. Eaton, Reynolds-number scaling of the flat-plate turbulent boundary layer, J. Fluid Mech. **422**, 319 (2000).
[85] I. Marusic, W. J. Baars, and N. Hutchins, Scaling of the streamwise turbulence intensity in the context of inner-outer interactions in wall turbulence, Phys. Rev. Fluids **2**, 100502 (2017).
[86] S. Toh and T. Itano, Interaction between a large-scale structure and near-wall structures in channel flow, J. Fluid Mech. **524**, 249 (1999).